crystals

MDPI

Article

Hydrogen Reduction of Tellurium Oxide in a Rotary Kiln, Initial Approaches for a Sustainable Process

Hanwen Chung, Semiramis Friedrich *, Mengqi Qu and Bernd Friedrich

IME Process Metallurgy and Metal Recycling, RWTH Aachen University, 52072 Aachen, Germany; hchung@ime-aachen.de (H.C.); bfriedrich@ime-aachen.de (B.F.)
* Correspondence: sfriedrich@ime-aachen.de

Abstract: In the recycling of semiconductor materials like Bi_2Te_3 or CdTe, TeO_2 may form as a by-product that can be directly reduced to recover metallic Te. The hydrogen reduction of TeO_2 offers an eco-friendly alternative to conventional carbothermic reduction by avoiding CO by-products. This study investigates the reduction of 99.99 wt.% purity level TeO_2 using hydrogen in an oscillating kiln furnace (200–800 °C, 2–7 h), with phase composition and microstructure analysed via XRD and SEM. Results demonstrate conversions of up to 89% (solid–gas) and 100% (liquid–gas), revealing that kinetics dominate over thermodynamics in controlling reaction progress. The work proposes a reaction mechanism based on morphological evolution observed in SEM images, suggesting that further parameter optimisation could enhance scalability. As the first lab-scale demonstration of hydrogen-assisted TeO_2 reduction, this study establishes a preliminary process window (temperature/time) and underscores the potential for industrial adoption. Future work should verify the proposed mechanism and refine operational parameters to maximize efficiency.

Keywords: hydrogen reduction; tellurium; tellurium dioxide; solid–gas reaction; semiconductor; thermoelectric materials

Academic Editors: Ziyuan Li and Yi Zhang

Received: 27 March 2025
Revised: 6 May 2025
Accepted: 12 May 2025
Published: 18 May 2025

Citation: Chung, H.; Friedrich, S.; Qu, M.; Friedrich, B. Hydrogen Reduction of Tellurium Oxide in a Rotary Kiln, Initial Approaches for a Sustainable Process. *Crystals* **2025**, *15*, 478. https://doi.org/10.3390/cryst15050478

1. Introduction

Tellurium (Te) has found its application in various areas, mainly the technological ones such as the semiconductor industry in the form of CdTe for manufacturing infrared detectors, and photovoltaic solar panels, as well as thermoelectric materials such as Bi_2Te_3 or Sb_2Te_3, used in refrigeration [1,2]. As the progression into circular economy is ascending, it is becoming worthwhile to focus on the less known but technological metals such as Te and its recycling. Tellurium is primarily found in copper ores as metal tellurides, such as copper telluride (Cu_2Te), along with noble metal tellurides, including Hessite (Ag_2Te) and Calaverite ($AuTe_2$). During the electrolytic refining of copper anodes in sulphate solutions, metallic impurities precipitate, forming a sludge enriched with platinum group metals (PGMs), Au, Ag, and Te [3]. The concentrations of Te and other impurities in this sludge vary significantly depending on the ore source. For commercial tellurium production, the sludge undergoes oxidative pressure leaching with dilute sulphuric acid to solubilize Te, followed by cementation with copper to yield Cu_2Te [4]. This intermediate product is subsequently processed via electrowinning to recover high-purity Te [5]. The primary production of Te is reported thoroughly by these authors [6], and when compared with possible secondary routes, it shows a much shorter and simpler process.

The situation in the secondary route looks different. While the recovery of Te from CdTe photovoltaic waste is a well-documented and industrially established process [7], not

many strategies have been reported so far to re-circulate Te from thermoelectric Bi_2Te_3 to support the re-manufacturing and re-application of the mentioned material. To address this gap, a comprehensive recycling strategy is being developed, integrating sequential stages of (1) mechanical disassembly/pre-treatment of waste materials, (2) hydrometallurgical processing for TeO_2 precipitation, (3) hydrogen reduction of TeO_2 to metallic tellurium, and (4) final metal refining [8]. This study specifically investigates the critical reduction step (Stage 3).

Several studies employed hydrometallurgical methods to treat Te-containing materials and produced TeO_2 [1,9–12]. The subsequent conversion of TeO_2 to Te remains underexplored in both the academic literature and industrial practice. This knowledge gap exists because TeO_2 typically occurs only as an intentionally produced intermediate rather than being a by-product from the conventional Te recovery, mostly through the copper route. Metallic Te can be produced from TeO_2 through two principal routes. The first one is a direct chemical reduction using sulphur dioxide (SO_2) in mineral acids (typically sulphuric or hydrochloric acid). While SO_2 is a powerful reducing agent, its toxicity, corrosiveness, environmental impact, and handling challenges often discourage industrial application [13]. The second one is a carbothermic reduction, leading to the formation of undesired CO_2 waste gas [14], contradictory to the EU's objectives [15].

Therefore, this paper proposes using hydrogen as the reducing agent with the corresponding reaction product of mostly H_2O [16], which is closer to environmentally friendly, carbon-free, or low-carbon processes.

Hydrogen energy is regarded as the most promising clean energy source in the 21st century by many countries due to its diversified sources, low carbon emissions, high efficiency, and wide range of applications [17]. It is renewable and does not produce harmful emissions when used in metal production. Utilising the environmental benefits, hydrogen metallurgy is a metallurgical process that uses hydrogen as a reducing agent or protective atmosphere [18]. One key benefit of hydrogen metallurgy is that hydrogen's unique atomic mobility facilitates rapid diffusion through the material. The high diffusion coefficient of hydrogen, which persists even at reduced temperatures, may also lead to catalytic effects by facilitating the formation of intermetallic hydrides in metals [18]. In addition, hydrogen as a protective atmosphere can effectively prevent certain metals from oxidising at high temperatures, as well as by-products such as sulphides or nitrides, thereby improving the purity and properties of metal products [19]. However, several disadvantages were also known and reported. The production cost of hydrogen, particularly 'green hydrogen', is high and can significantly influence the total cost of hydrogen-produced metal. Regardless of producing hydrogen from natural gas steam reforming or electrolysis, the processes are very energy-intensive and can lead to possible considerations of green electricity availability [18,20,21].

Other than steel production, the usage of hydrogen in modern metallurgical processes enabled the efficient extraction, refining, and recycling of metals. Figure 1 outlines key applications across three domains: pyrometallurgy, hydrometallurgy, and plasma metallurgy.

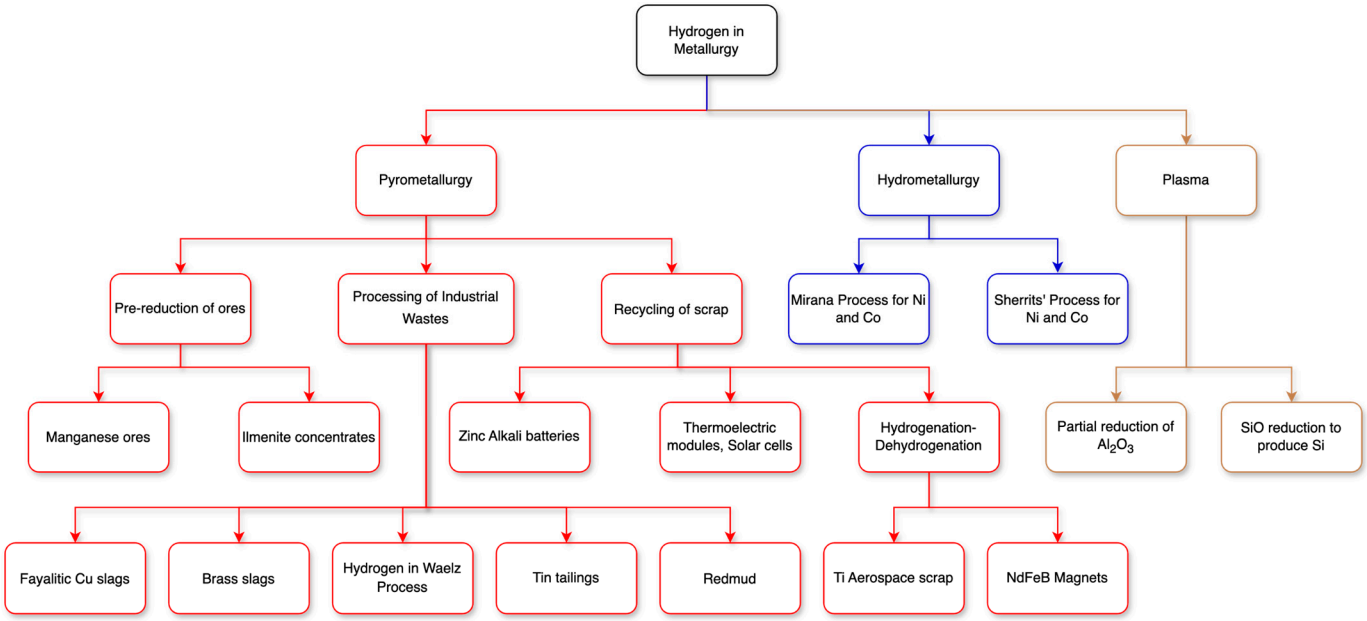

Figure 1. Application of hydrogen (as H_2/H) in metallurgy [22,23], modified.

Using hydrogen specifically as reducing agent has also been intensively studied and researched on non-ferrous metals such as Cu [24], Ni [25], Mo [26], V [27], Ge [28], Bi [29], Sn [30] and waste systems such as bauxite residue [31], copper smelting slag [32], and brass converter slag [33]. In these studies, the reaction products contain only H_2O as a by-product. On the reduction process, there are further thermodynamic benefits, as hydrogen reduction occurs at significantly lower temperatures, requiring less energy to reach reaction temperatures. Its exceptional selectivity enables precise metal recovery from complex feedstocks like battery waste and copper slags [22]. Further information on the industrial applications of hydrogen in extractive metallurgy can be found in the review by Tang et al., Rukini et al., and Luidold et al. [18,34,35].

While hydrogen reduction of TeO_2 for metallic Te is not a common target, the process is not entirely unprecedented. The kinetics of this reaction has been studied and characterised by Trawinski et al. with the aim of synthesising bismuth telluride (Bi_2Te_3) [29,36,37]. In that study, thermogravimetric analyses were conducted under non-isothermal conditions with heating rates varying between 2 and 6 K/min. The results suggested an optimal reaction temperature around 715K, i.e., slightly below the melting temperature of Te (723K). The authors proposed that the melting point might be even lower due to the nanoscale size of their Te particles. Furthermore, a thermal function was also obtained from the kinetic analysis, which calculated the activation energy to be 69.2 kJ/mol. Although the kinetic characterisation was aimed at synthesising Bi_2Te_3, the work established a foundation for scaling up the reduction process.

Hydrogen reduction has demonstrated significant potential in micro-scale studies, including kinetic investigations by Trawinski, but its scalability and feasibility in industrial settings remain underexplored. To bridge this gap, the present study investigates the application of hydrogen reduction within a rotary kiln system, aiming to evaluate the engineering feasibility and operational parameters of this process. Rotary kilns are well-suited for studying gas–solid reactions due to their widespread industrial use in processes such as limestone calcination, cement production, and zinc calcination [38,39]. The state-of-the-art technology for gas–solid reactions allows efficient heat and mass transfer up to high temperatures, making them ideal for experimental research.

2. Materials and Methods

Prior to the experimental trials, the thermodynamic feasibility of the reaction was assessed using FactSage 8.0, a thermochemical modelling software. This was further supported by DTA-TGA to confirm the endothermic/exothermic events and provide baseline data. For the experimental trials, synthetic oxide powders were used instead of actual recycled materials. The experimental procedure starts with characterising the initial materials (99.99 wt.% TeO_2 from Wuhan Tuocai Technology Co., Ltd., Wuhan, China). The chemical composition was analysed using ICP-OES. The phase composition of the TeO_2 powder was analysed using X-ray diffraction XRD with Cr-radiation. The average particle size of the powders was measured using a laser particle size analyser, and particle morphology was filmed using SEM imaging.

The reduction process was carried out in a rotary kiln reactor furnace, equipped with a quartz kiln tube (model TSO 1-11/400, Carbolite Gero GmbH & Co. KG, Neuhausen, Germany). Unlike a conventional rotary kiln, this reactor is moved just by oscillating up to 314° in each forward and reverse direction at 1–8 oscillations per minute. While the oscillatory motion of the laboratory-scale apparatus differs from the continuous rotation of industrial rotary kilns, this configuration is a suitable approach for experimenting thermal and material transport phenomena under controlled conditions. Its widespread adoption in small-scale studies is justified by its ability to replicate key process dynamics, such as heat transfer and reactant mixing, which remain critical to understanding kiln-based systems.

The oscillatory motion enabled increasing the contact surface area between the TeO_2 powder and the reactive gas, hydrogen. The gas flow was controlled and monitored using a gas control system, and the hot output gas after the reaction was passed through a bottle of distilled water to be cooled down. The experimental setup is shown in Figure 2.

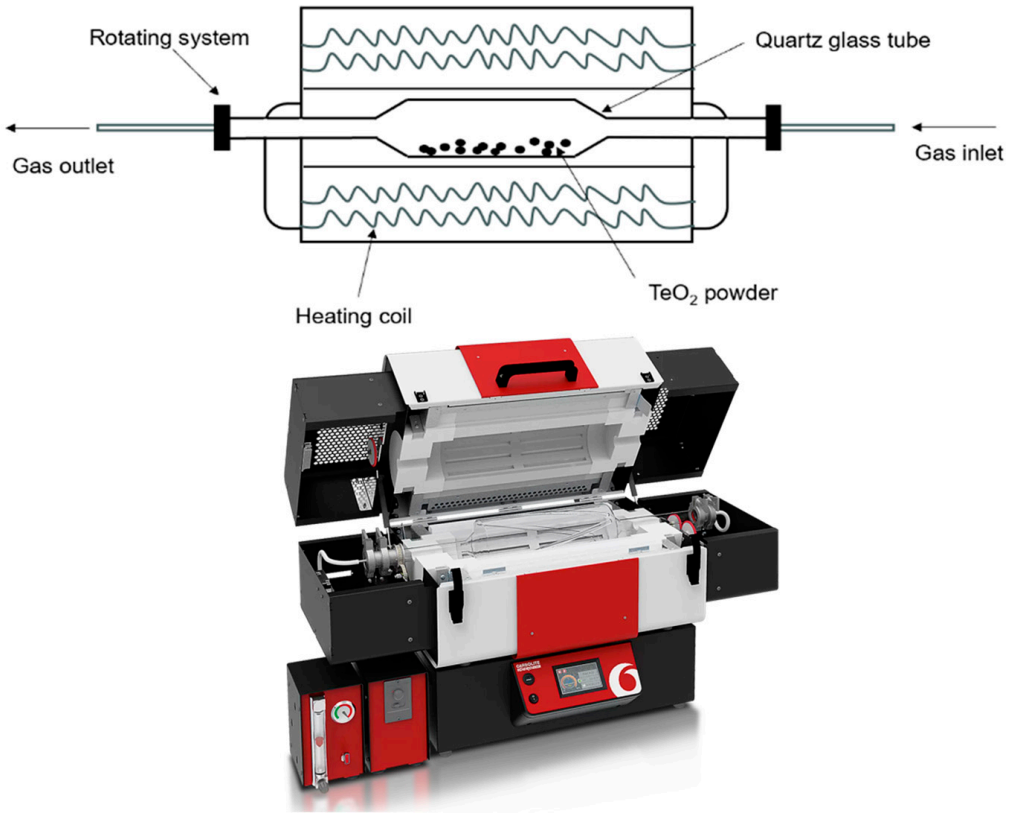

Figure 2. Experimental setup for the hydrogen reduction of TeO_2, (**top**) schematic illustration and (**bottom**) furnace setup.

After loading roughly 100 g of as-purchased material, the quartz glass kiln tube was flushed with Ar gas to remove any air and then heated to the set temperature. Once the temperature reached the predetermined value (compare Table 1), high-purity hydrogen gas (5.0) was introduced into the kiln tube at intervals with a flow rate of 1 L/min. The total gas flow duration was adjusted based on the stoichiometric requirement for the reaction, ensuring sufficient gas supply throughout the holding time. Since the kiln tube is open-ended, introducing the gas at intervals ensured sufficient dwell time for the hydrogen gas to react with the powder. To compensate for any potential insufficient contact between the particles and the gas, the total amount of hydrogen used was always at least 1.5 times the stoichiometric requirements. After the holding time, the kiln tube was flushed with Ar gas to remove any remaining water vapour and hydrogen gas. Following, the furnace was simply switched off and allowed to cool naturally to ambient temperature without active cooling measures or temperature ramping. Before determining the mass change, the kiln tube was flushed again with Ar gas to remove any residual hydrogen. According to the weight loss of the material and the Equation (5), the conversion was calculated. The reaction products were collected and analysed using quantitative XRD as well as SEM/EDS. The experiments were conducted over a temperature range of 200 to 800 °C, with holding times varying from 2 to 7 h.

Table 1. List of experimental trials with temperature and holding time as parameters.

Test	Temperature [°C]	Holding Time [h]
1	200	2
2	200	4
3	300	2
4	300	4
5	425	4
6	425	5
7	425	6
8	425	7
9	450	4
10	500	2
11	500	3
12	700	4
13	800	2

3. Results and Discussion

3.1. Thermodynamic Calculations Using FactSage 8.0

Using the Richardson–Ellingham diagram, which reflects the thermodynamics of metal oxidation and reduction, the formation lines of TeO_2 and H_2O have been illustrated in Figure 3. These lines are calculated with the *Reaction* function in FactSage 8.0 with FactPS and FTOxid database, using an activity coefficient of 1 in all calculations. Within the diagram, it can be seen that a reduction of TeO_2 with hydrogen is feasible, as the values show that hydrogen has a stronger chemical affinity with oxygen, and its oxidation line is located below that of TeO_2 formation.

In addition to being environmentally friendly, hydrogen reduction also has the thermodynamic advantage over carbon as a reducing agent. A hypothesised hydrogen reduction of TeO_2, producing Te and H_2O, is expressed in Equation (1), and the ΔG^0 is expressed by Equation (3). For comparison purposes, the carbothermic reduction of TeO_2 is shown in Equation (2) and the ΔG^0 in Equation (4). These Equations are obtained similarly from FactSage. Both reactions have confirmed the thermodynamic feasibility of the reaction, as

well as the required temperature and its spontaneity. Despite the two possible pathways, the hydrogen reduction is shown to be more favourable thermodynamically (see Figure 4).

$$2\ H_2\ (g) + TeO_2\ (s) \rightarrow Te\ (s) + 2\ H_2O\ (g) \quad (1)$$

$$C\ (s) + TeO_2\ (s) \rightarrow Te\ (s) + 2\ CO_2\ (g) \quad (2)$$

$$\Delta G^0 = 3\times10^{-5}T^2 - 0.1065T - 158.55 \quad (3)$$

$$\Delta G^0 = -0.3546T - 100.7 \quad (4)$$

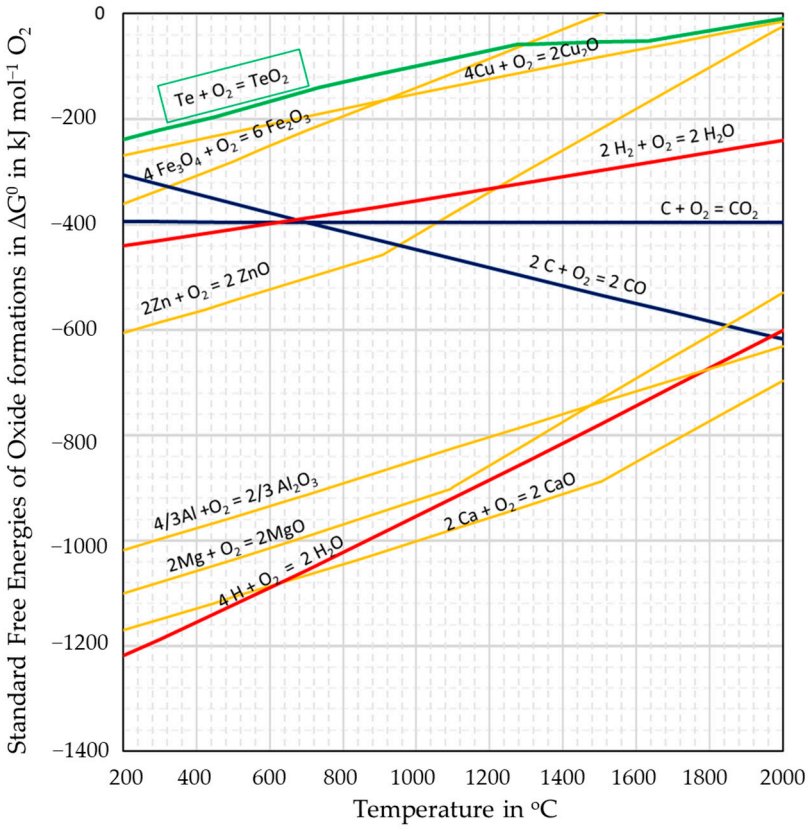

Figure 3. Richardson–Ellingham diagram with TeO_2 and H_2O formation.

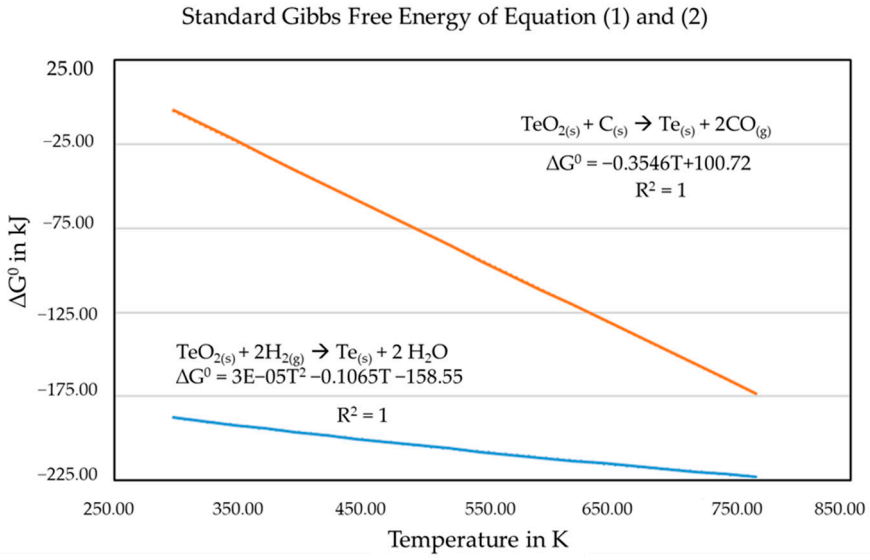

Figure 4. Standard Gibbs free energy of Equations (1) and (2).

The hydrogen reduction in the TeO_2, according to Equation (1), has been calculated for its possible product formation based on thermodynamic considerations, and the results are shown in Figure 5, which shows that the reaction between TeO_2 and H_2 can happen already at room temperature. At elevated temperatures up to 450 °C, common impurities including Pb, Bi, Cu, Se and Ag may form solid compounds with Te, such as PbTe, Bi_2Te_3, CuTe, and Ag_2Te, that may contaminate the metallic Te.

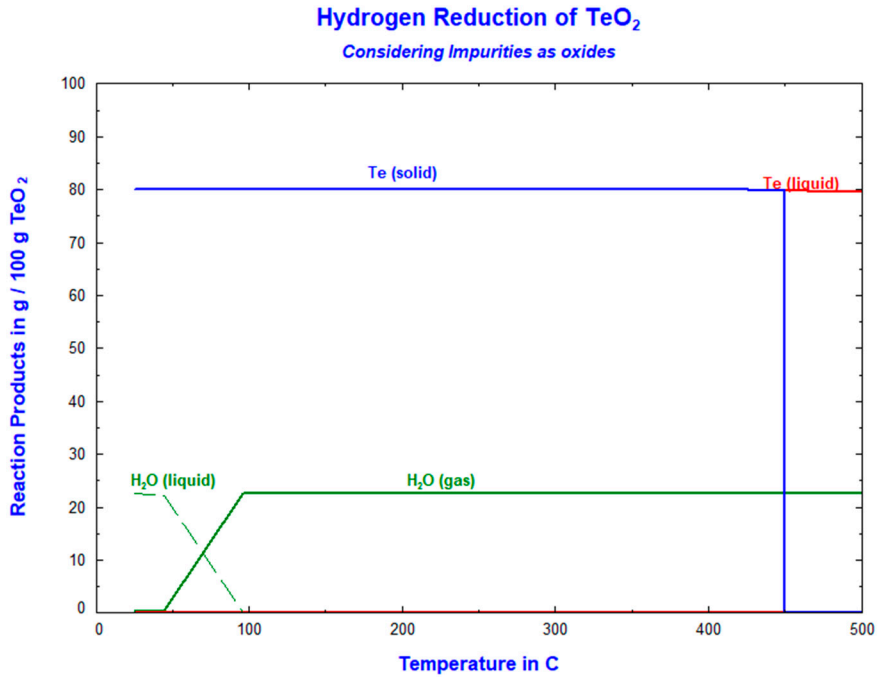

Figure 5. Calculated main products for the reduction of TeO_2.

Additionally, trace amounts of PbSe, CuSe, and Bi_2Se_3 can also form but at insignificant ranges lower than 0.01% that would hardly affect the reduction process. From the results and the Equation (1), a complete reduction of the input materials reduces the total solid weight by 20.05 g/100 g TeO_2. Thus, the mass balance method to quantify the conversion rate, α, with the following Equation (5) can be used for further evaluation in this current study.

$$\alpha = \frac{m_{loss}}{20.05\% \times m_{input}} \times 100\% \quad (5)$$

3.2. Differential Thermal Analysis and Thermo-Gravimetric Analysis

To validate the thermodynamic calculations obtained from FactSage in Chapter 2, differential thermal analysis (DTA) as well as thermogravimetric analysis (TGA) were conducted using a simultaneous thermal analyser to characterise the reduction behaviour of TeO_2 under hydrogen atmosphere. For this purpose, a hydrogen gas flow rate of 5 L/h and a gas purity level of 5.0 were set. The powder was then heated up from 15 °C to 430 °C and kept for a dwelling time of 960 min at that temperature. This temperature was selected to remain below the melting point of Te. Finally, the system was just turned off. The recorded temperature and mass changes progression have been represented in Figure 6. It can be seen that during the heating period, a slight exothermic effect was observed around 300 °C, which is attributed to the hydrogen reduction of TeO_2, as indicated by the relative enthalpy change of −610.79 J/g. The total mass loss of 24.43% depicts that TeO_2 has been completely reduced to metallic Te, as this exceeds the theoretical value of 20.05%. This excess of mass loss is likely due to the volatilisation of metallic Te. These DTA results not only confirm the feasibility of hydrogen reduction in TeO_2, but also define the first process

window for the trials. In this study, the temperature and holding time have been further investigated to optimise the conversion.

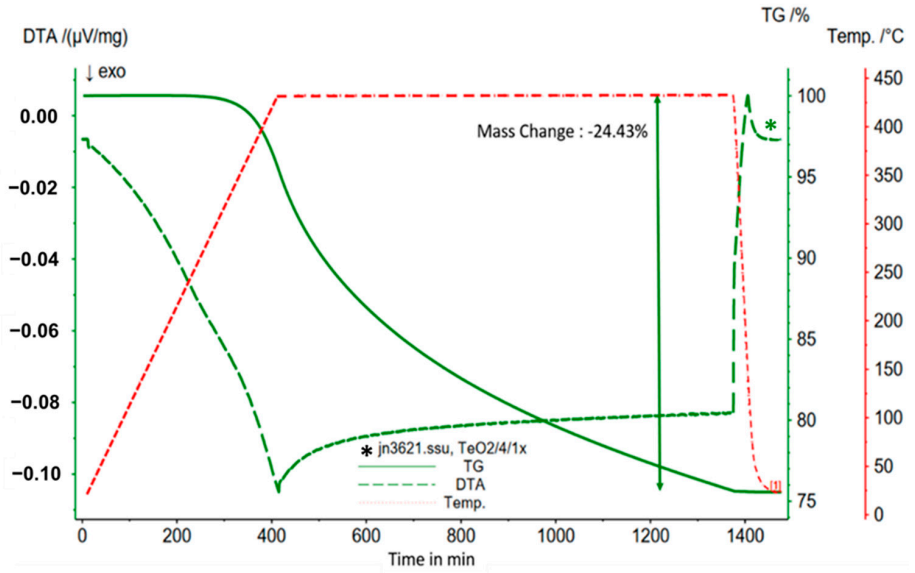

Figure 6. Mass change (TG), DTA signal (DTA), and temperature (Temp.) of the TeO_2 sample in relation to time.

3.3. Materials Characterisation

The chemical composition of the TeO_2 powders can be seen in Table 2, as well as its XRD pattern in Figure 7. The TeO_2 powders have a relatively high specific surface area of 0.453 m^2/g and may enhance reaction kinetics in the reduction process. The uniformity index of 0.557 indicates moderate variation in the particle sizes that could help exclude low conversion due to differences in size. Detailed particle size distribution has been illustrated in Figure 8.

Table 2. Chemical composition of TeO_2 (99.99 wt.%) by ICP-OES, in ppm.

Ag	Al	Ca	Fe	Mg	Na	Si	Cu	Se	Pb	Bi
0.18	0.35	6.55	0.90	0.15	3.25	21.85	6.25	6.25	6.25	8.75

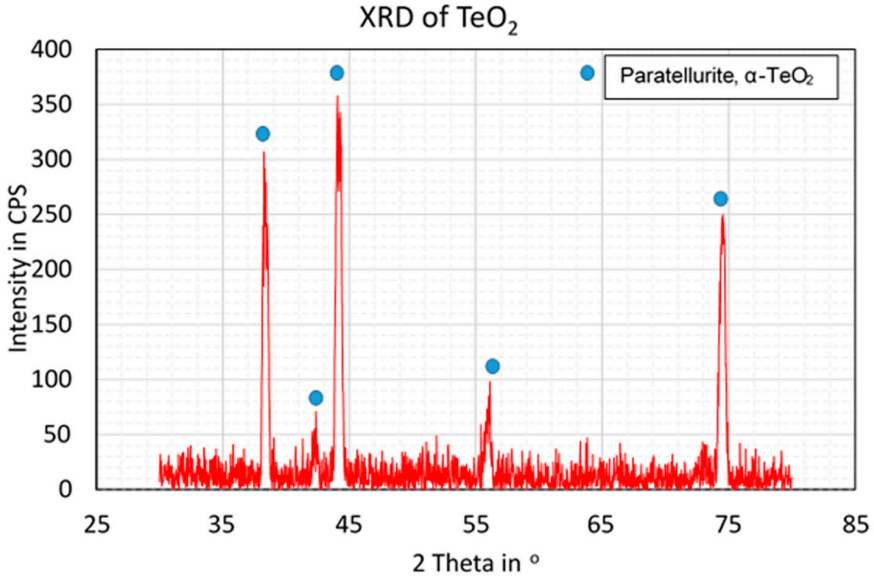

Figure 7. XRD pattern of TeO_2 powder, used in this work.

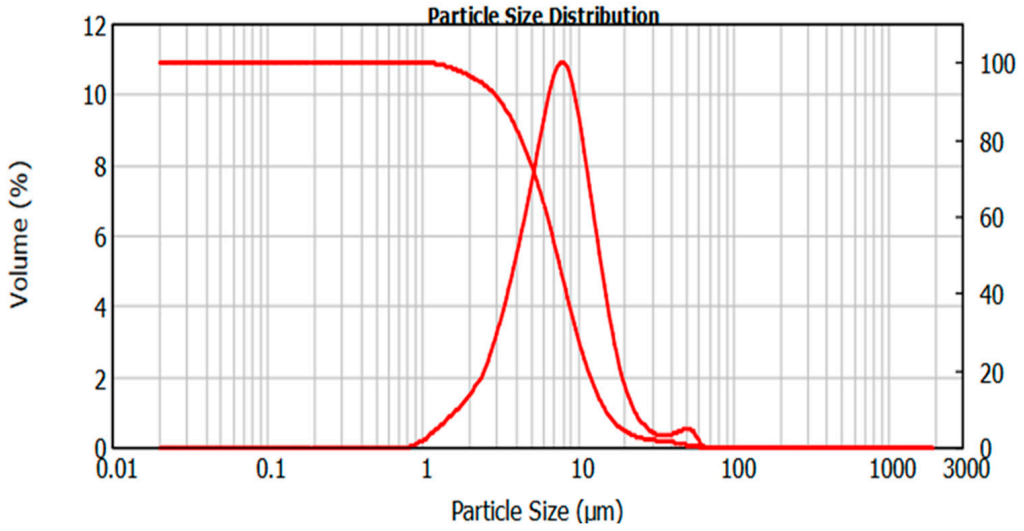

Figure 8. Particle size distribution of TeO_2 powder, used in this work.

3.4. Reduction of TeO_2

The amount of TeO_2 reduced for all experiments was calculated with Equation (5), and the results in relation to temperature, holding time, and conversion are shown in Figure 9 below. To further quantify the amount of metallic Te in the end product, the following Equation (6) can be applied by considering the total input mass, m_{input}, total output mass, m_{output}, and the molar mass ratio of Te to TeO_2.

$$\%Te_{metallic} = \alpha \times \frac{m_{input}}{m_{output}} \times \frac{127.6}{159.6} \times 100\% \quad (6)$$

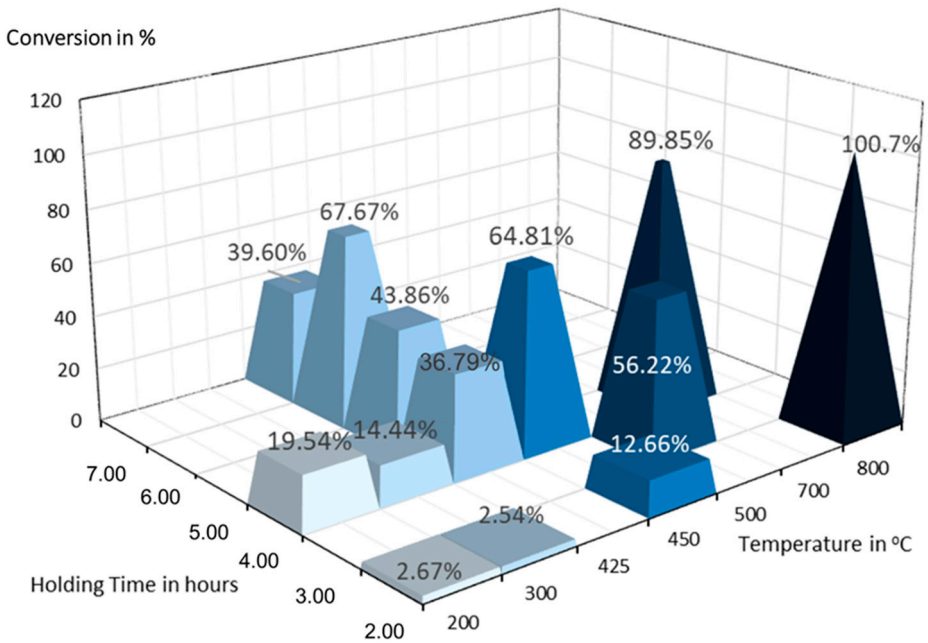

Figure 9. Temperature and holding-time-dependent conversion of TeO_2.

Theoretical FactSage calculations, as shown in Figure 5, indicate that the reactions should be thermodynamically feasible well below the melting point of Te. To verify this, two sets of experiments were conducted at 200 °C and 300 °C with holding times of two and four hours. The results revealed low conversion rates, up to 19.5%, confirming that the hydrogen reduction in TeO_2 is strongly limited by reaction kinetics, despite the

relatively low activation energy and the use of fine-grained initial particles. Despite the unexpected trends in conversion rates at 200 °C and 300 °C for four hours, the effect of temperature increase has a stronger and positive influence on the reaction kinetics than on the thermodynamics. This was further demonstrated at higher temperature ranges above the melting point of Te, specifically at 450 °C, 500 °C, and 700 °C. At these temperatures, significantly higher conversion was observed, emphasising the importance of kinetics over thermodynamics. Post-experimental observations at 450 °C and 500 °C revealed similar black powders distributed throughout the kiln tube. At 700 °C, a metallic layer was observed covering the inner wall of the glass kiln tube (Figure 10a), along with a mixture of fine pellets (radius < 2 mm) and powders. This can be attributed to the stronger melting of Te, which likely reduced adhesion to unreacted particles, thereby enhancing the interaction between oxides and the reducing gas, resulting in a much higher conversion.

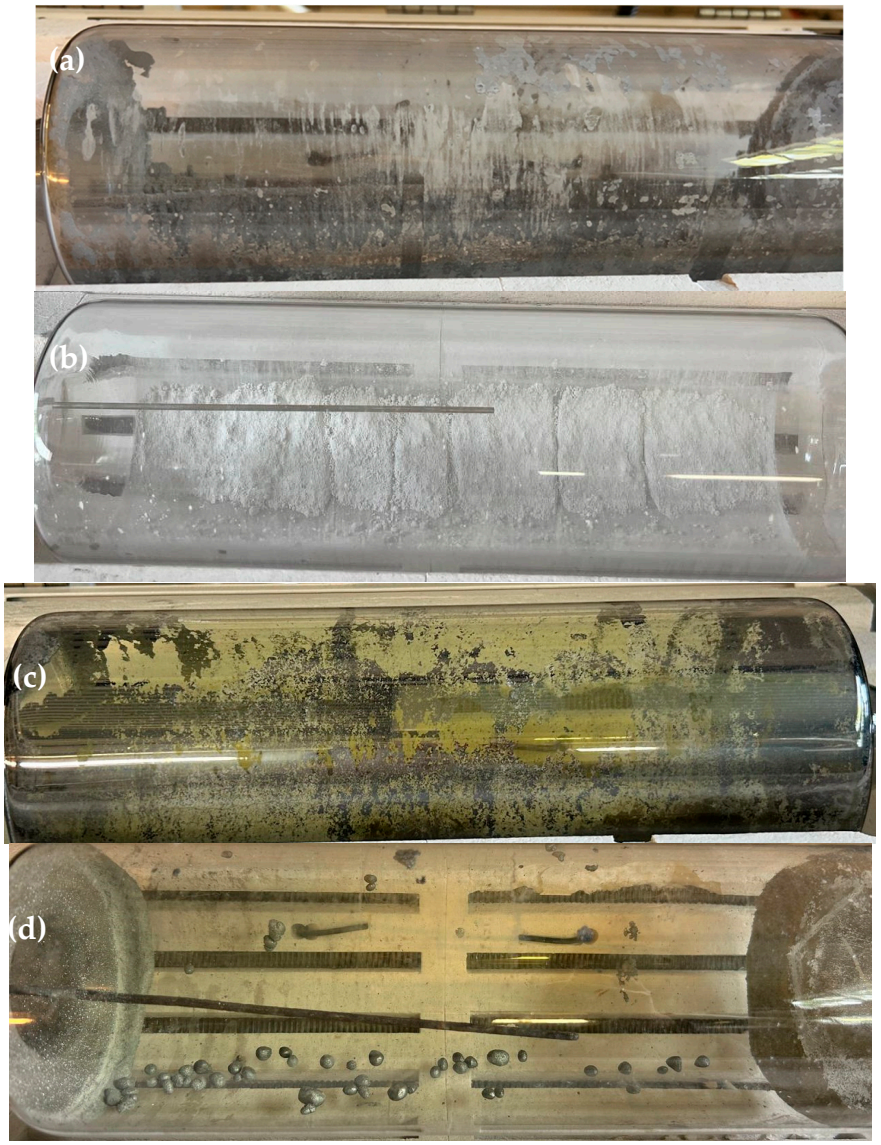

Figure 10. (**a**) Thin metallic layer after reduction at 700 °C, (**b**) materials within the glass kiln tube before reduction, (**c**) after 6 h reduction at 425 °C, (**d**) after 7 h reduction at 425 °C.

For further investigation, experiments were conducted at a temperature of 425 °C with holding times of 4, 5, 6, and 7 h. These parameters were chosen based on DTA-TGA results

and practical experimental considerations. An expected increasing trend in the conversion was observed, rising from 36.79% at 4 h to 67.67% at 6 h.

However, the conversion at 7 h did not follow the expected increasing trend, dropping to 39.60%. This anomaly is likely due to the formation of metal layers that fully coated the oxide particles over time, resulting in the formation of pellets with radii of less than 10 mm, as shown in Figure 10. The pellet formation may have been facilitated by the presence of water vapour, which can act as a binding agent for both the reacted and unreacted materials. These pellets likely hindered gas diffusion, effectively reducing the conversion. This observation contrasts with the results at 6 h, where the reaction products were evenly distributed throughout the glass kiln tube without pellet formation. This difference could be due to a high H_2O ratio, likely resulting from the intermittent exhaustion of the system, as water vapour ratio control was not considered in this study.

To further investigate the process, a liquid–gas reduction experiment was conducted at 800 °C. As this temperature has been above the melting point of TeO_2 (T_m = 723 °C), the challenge of ensuring sufficient interaction between hydrogen gas and the oxide particles could be eliminated, leading to the complete reduction of the oxides. Due to the evaporation of metal, the recorded mass loss and conversion exceeded 100%. After only two hours of process dwelling time, a metallic bar was obtained (see Figure 11), whose chemical composition, analysed by XRD, is shown in Figure 12.

Figure 11. Reaction products after reducing at 800 °C for 2 h.

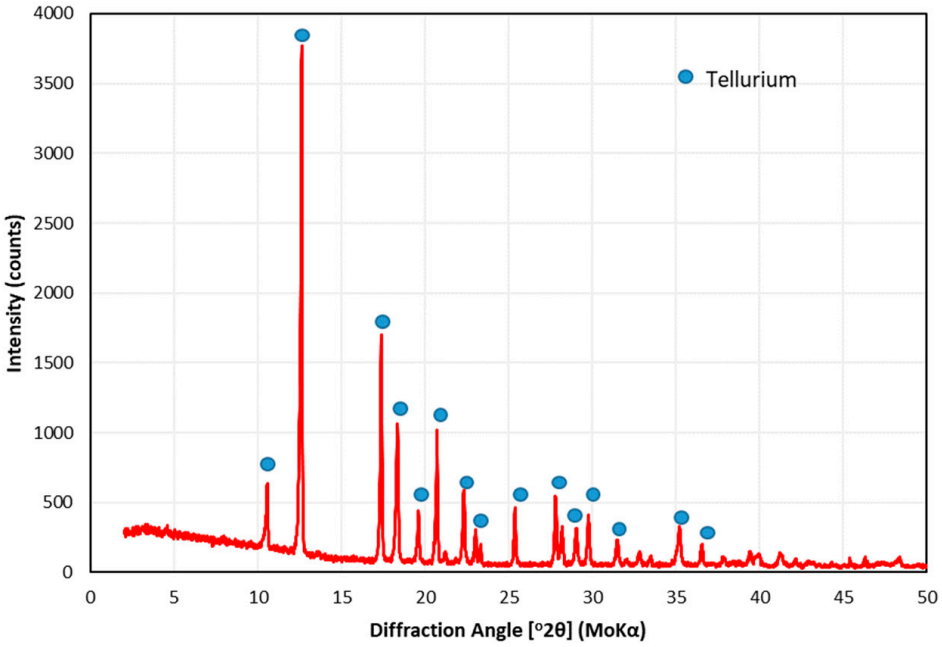

Figure 12. XRD peaks of the reaction products after two hours dwelling at 800 °C.

It should be noted that the recorded mass loss may include a very small percentage of volatilised metallic Te. The volatilised Te could either be transported out of the glass kiln tube by the intermittent flow of water vapour and hydrogen gases or adhere to the oxide or metallic particles inside the glass kiln tube when the H_2O ratio is sufficiently high. The latter scenario is considered more likely, as the experimental setup only allows gas to exit the kiln tube under overpressure conditions or when the input gas flow is active.

Since the conversion is derived through mass balance calculations, which may exhibit significant sensitivity and potential sources of systematic error, it is essential to validate these results by comparing the conversion and the formed phases to ensure their accuracy and reliability. For this, two samples were analysed with a Rietveld-Refined XRD analysis, a method for quantitative phase analysis, as seen in Table 3. Sample P1 underwent five hours dwelling at 425 °C, and sample P2 underwent four hours dwelling at 200 °C. These two samples have minimal and moderate conversion by mass balance calculation, allowing for a clearer assessment of the phase composition.

Table 3. Quantitative analysis of 2 selected samples.

Sample	Conversion by Mass Balance	Theoretical $Te_{metallic}$	Phase Composition by XRD	
			Te	TeO_2
P1	43.09%	37.57%	43.5%	56.5%
P2	19.54%	16.17%	18.1%	81.9%

The XRD pattern includes two phases: TeO_2 (Paratellurite) and tellurium (Te). The theoretical values according to Equation (6) were calculated to be 37.57% for P1 and 16.17% for P2, while the measured values were 43.5% (P1) and 18.1% (P2), respectively (compare Figure 13). Although there is a variation between the theoretical and measured values, the calculated error of approximately 15% and 12% is deemed to be within an acceptable range, considering multiple sources of error.

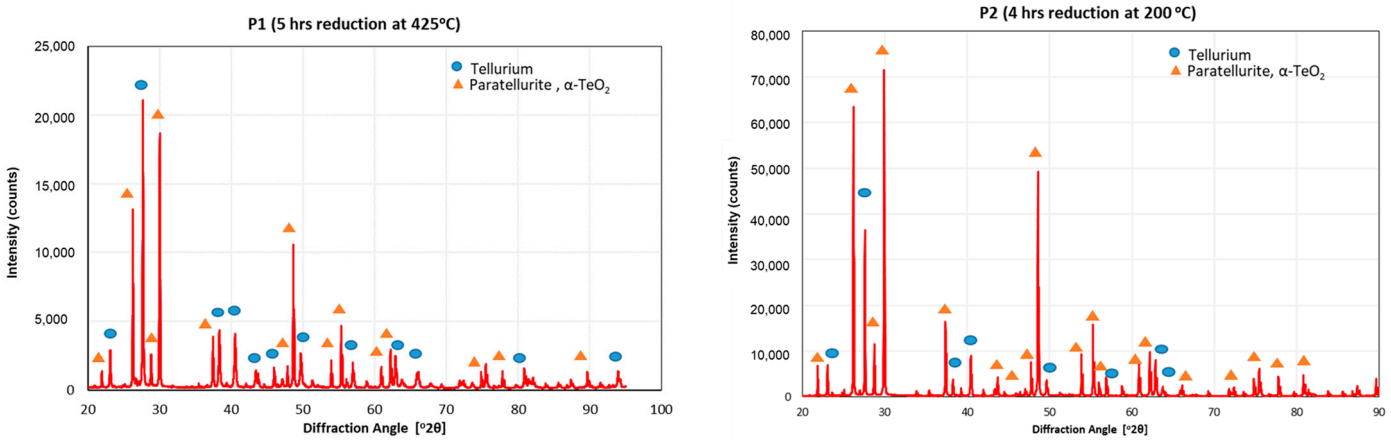

Figure 13. Rietveld-refined XRD analysis of (**left**) sample P1, (**right**) sample P2.

The first source of error lies in the Rietveld refinement process, which yielded a goodness-of-fit (GoF) value of approximately 2, suggesting that further optimisation may improve the fit. Additionally, the inhomogeneity of the samples, as evidenced by the SEM images presented in Chapter 3, contributes to the observed deviations. Despite these variations, the results remain valid for assessing the use of the mass balance method, as the primary objective is to confirm its applicability rather than achieve exact numerical agreement.

3.5. Microscopic Analysis

In order to investigate the kinetic mechanism of the reduction in each oxide particle, some selected samples were analysed using a scanning electron microscope (SEM). The starting material, as shown in Figure 14, revealed that the powders had an irregular, quasi-geoidal shape, with rough and uneven surfaces. These geometries indicate that the powder may be more prone to agglomeration in the process. Given the coexistence of metallic Tellurium and residual TeO_2, sample P1 with a conversion of 43% was selected for this investigation. This selection allowed for better differentiation between the two phases. Energy Dispersive Spectroscopy (EDS/EDAX) was also conducted alongside SEM to analyse the elemental composition of the sample. The results of the EDS analysis (compare Figure 15) support the distinction between the Te and TeO_2 phases observed in the SEM images, while the SEM images, shown in Figure 14, reveal distinct changes in the sample's particle structure resulting from the hydrogen reduction. These observations provided critical insights that contributed to the development of a possible reduction mechanism, which is illustrated in Figure 16 and discussed in further detail below.

The reduction process begins when hydrogen gas encounters TeO_2 particles. During the transformation, shrinkage and pore development can be observed in Figure 14c, with metallic Te separating from the main particle as Te nuclei. These nuclei appear as tiny, scattered white spots, as shown in Figure 14d, and were verified by EDS (Point 2). As the reaction progresses, the individual nuclei begin clustering into larger, denser structures, initiating nucleation, while other oxide particles continue to react simultaneously (Figure 14e). During nucleation, oxide particles, regardless of their degree of reduction, may gather around and attach to the growing crystals (Figure 14f). This could lead to the entrapment of unreacted particles within the crystal, resulting in incomplete reduction of the total mass. This observation may explain the less than 100% conversion observed in all experiments below the melting temperature, regardless of temperature and holding time. In Figure 14g, clumps of crystals and oxide particles are visible at multiple points. However, oxide-particle-free crystals are also seen in Figure 14h, indicating that entrapment and clumping do not occur uniformly, which could be due to the oscillating movement of the equipment.

The exact mechanism may resemble a typical gas–solid reaction, involving adsorption, surface reaction, desorption of reaction by-products (such as H_2O gas due to high temperature), and the transformation of metal oxides into metal. However, this exact process could not be directly verified in this study because the proposed mechanism requires further validation. Specifically, the reaction pathway and rate-limiting steps remain uncertain. Furthermore, it may be possible to determine the mechanism more precisely by fitting experimental data into model Equations, such as the Avrami–Erofeev model [40], diffusion-controlled models, or the interface-controlled shrinking core model [41]. However, such detailed kinetic modelling and analysis are beyond the scope of this work.

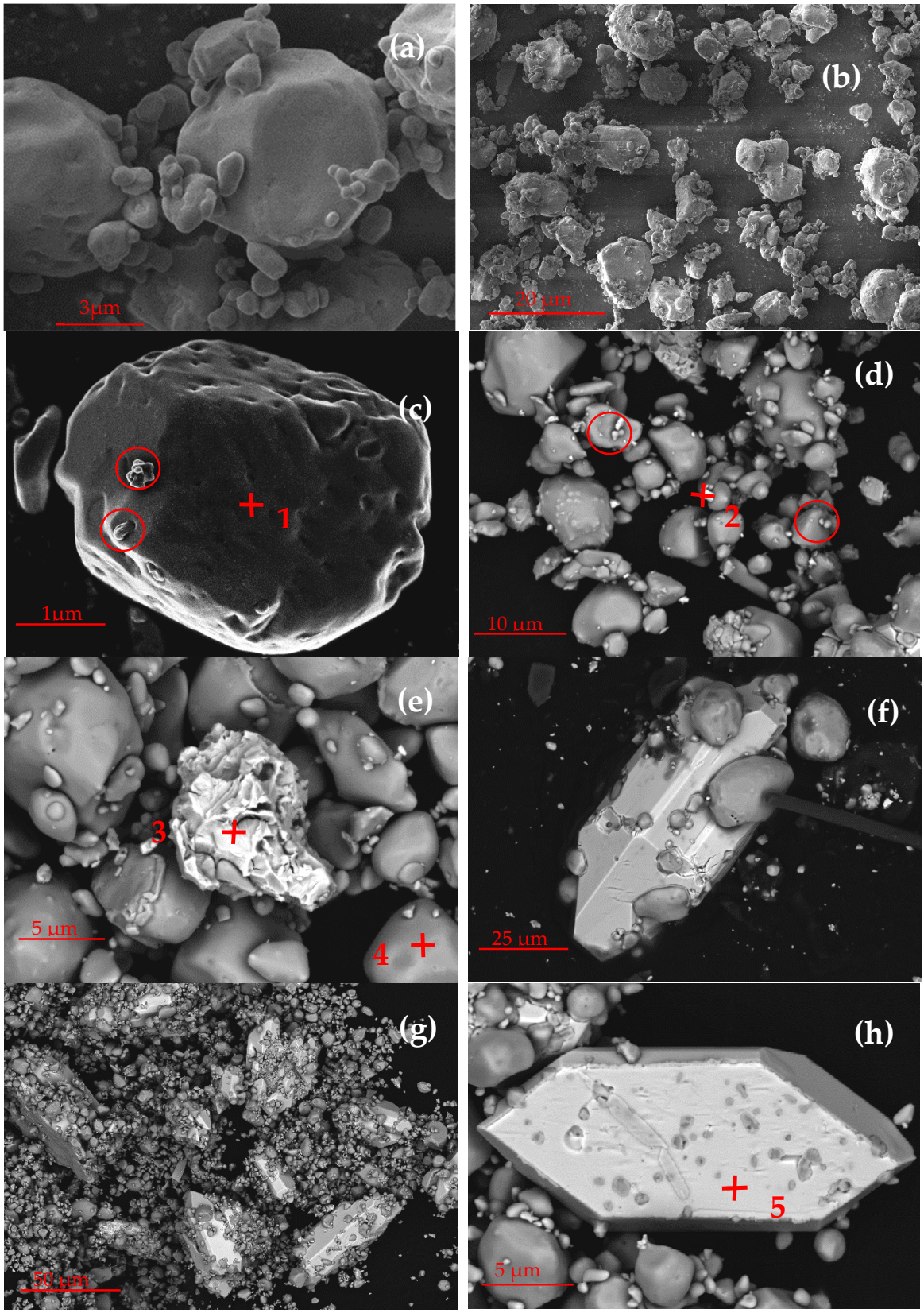

Figure 14. SEM images showing—(**a**) unreacted TeO_2 particles at 20,000× and (**b**) 3500× magnification, (**c**) TeO_2 particle with pore formation, shrinkage and reduced metal marked in red circle, (**d**) TeO_2 particle with scattered Te nucleus marked in red circle, (**e**) clustering and nucleation of Te, (**f**) entrapment of oxide particles around the metal crystal, (**g**) clumps of oxide and crystals, (**h**) oxide-particle-free crystal with traces of gold powder for the SEM imaging.

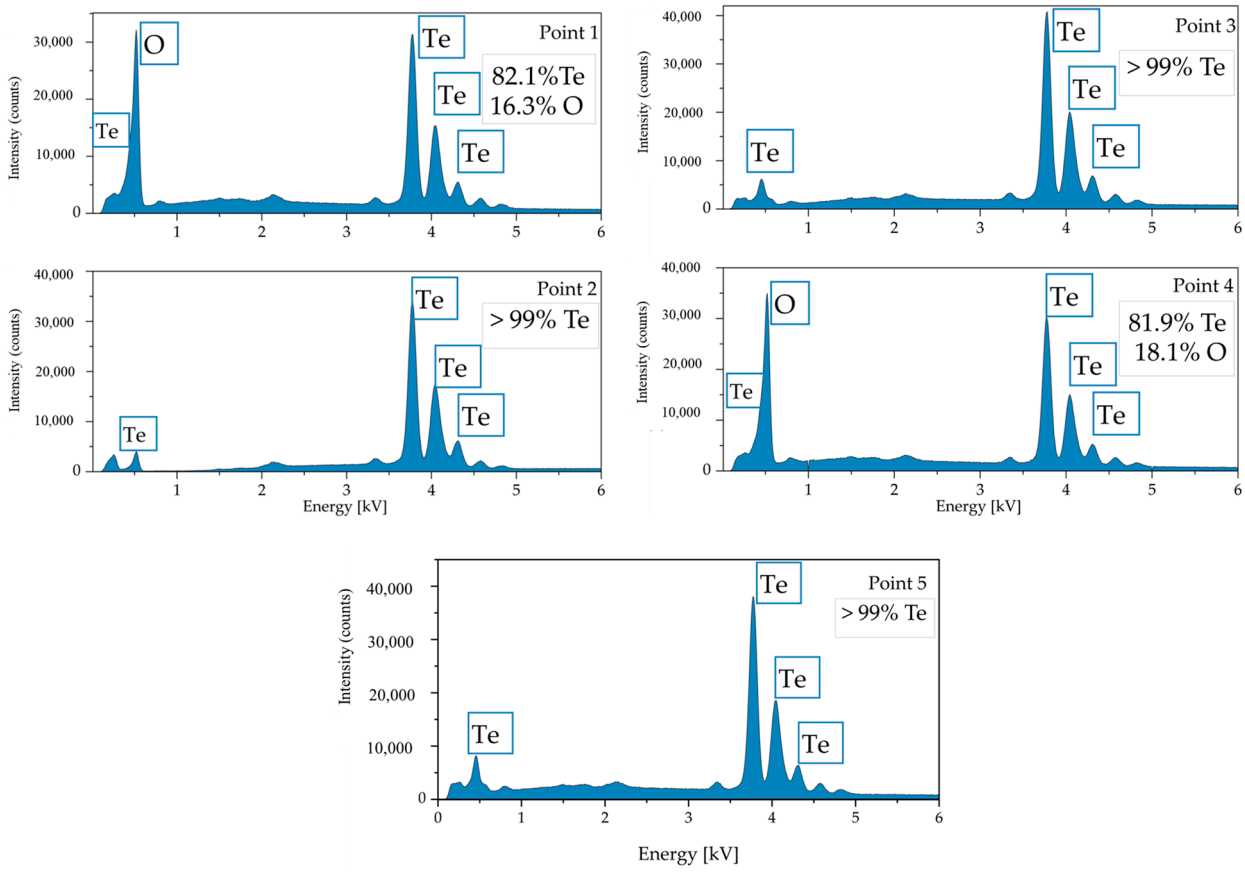

Figure 15. EDS signals of point(s) 1–5 indicated with normalised result.

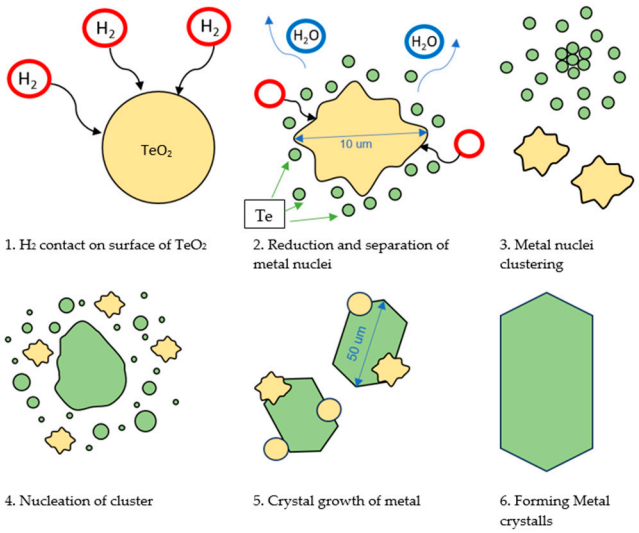

Figure 16. Proposed reduction mechanism according to the nucleation model with possible pore formation from [18].

4. Conclusions

Within the broader context of developing Te circularity, a framework for treating Bi_2Te_3 waste through four potential processing steps has been conceptualised. This paper focuses on experimentally validating one critical step—the reduction in TeO_2 to metallic Te. To ensure environmental sustainability in this reduction process, hydrogen has been selected as the reducing agent, avoiding the drawbacks associated with conventional reductants like C or SO_2.

This feasibility study explored a reduction process inside a rotary kiln, focusing on optimising the metallurgical process through parameter study to enhance its productivity. The results yielded several key findings: (1) The hydrogen reduction pathway has been experimentally validated as an effective approach inside the rotary kiln, though further optimisation is required to enhance efficiency. Achieving a complete reduction in solid–gas reactions is challenging due to the entrapment of unreacted oxide particles within the reduced metal, as seen in the SEM images. (2) The kinetics of the reaction significantly influence the reduction process, as evidenced by low conversion at low temperatures (200 °C and 300 °C) despite favourable thermodynamics ($\Delta G^\circ < 0$ for $TeO_2 + H_2 \rightarrow Te + H_2O$ even at 200 °C). (3) A direct and efficient approach for producing metallic Te from TeO_2 is achieved by first melting the oxide at 800 °C before reacting it with hydrogen inside the rotary kiln, thereby enabling a 100% conversion via liquid–gas reaction. This suggests that higher temperatures, which may induce melting or evaporation of the reduced metal, could facilitate the reduction process. (4) A reduction mechanism was proposed based on SEM images and established principles of solid–gas reactions, providing a basis for further investigation into the production of Te from TeO_2.

These findings collectively demonstrate progress in the recycling of Te, e.g., from semiconductor materials, addressing the critical step of obtaining metallic Te. However, as this is an initial approach for the process, the number of replicates for each experimental condition is insufficient to provide in-depth statistical results to strengthen the interpretation. The study is also limited by the lack of precise control over the H_2O/H_2 ratio in the solid–gas reaction, highlighting the need for further optimisation. The optimisation needs to address the kinetic limitations rather than just thermodynamic feasibility. This can be achieved by improving the equipment design, particularly by enhancing particle–gas mixing within the rotary kiln. Follow-up work should focus on refining the parameters and exploring alternative configurations, potentially under elevated hydrogen pressures, to further improve the efficiency and yield of the reduction process. Lastly, kinetic analysis (e.g., isothermal and isoconversional analysis of TGA data) should be conducted to verify the reaction mechanism.

This process, described in this study, has achieved technology readiness level (TRL) 3, demonstrating experimental proof of concept in a laboratory environment. To further assess the maturity of the process, it is necessary to address additional considerations such as energy consumption and real-time gas composition monitoring, e.g., with mass spectrometry. Subsequent studies should also integrate other steps in the conceptual framework. The success of the conceptual framework should then provide insights on adaptability for other elements beyond Te, including chemically similar chalcogenide compounds.

Author Contributions: Conceptualization, H.C.; methodology, H.C. and S.F.; software, H.C.; validation, H.C. and S.F.; formal analysis, H.C. and M.Q.; investigation, H.C. and M.Q.; resources, B.F.; data curation, H.C. and M.Q.; writing—original draft preparation, H.C.; writing—review and editing, S.F.; visualisation, H.C. and M.Q.; supervision, S.F. and B.F.; project administration, S.F.; funding acquisition, B.F. All authors have read and agreed to the published version of the manuscript.

Funding: This research was funded by the Federal Ministry for Economic Affairs and Climate Action of Germany (Bundesministerium für Wirtschaft und Klimaschutz), grant number 03EN2056C.

Data Availability Statement: The data supporting the findings of this study are part of the RecycleTEAM project and are not publicly available at this time. Access to the data may be granted upon reasonable request and approval from the RecycleTEAM project administrators.

Conflicts of Interest: The authors declare no conflicts of interest.

References

1. Zhang, H.; Li, Z.; Yang, Y.; Zha, G.; Xu, B.; Liu, D.; Yang, B.; Jiang, W. Advances in tellurium recovery and purification: A comprehensive review of separation methods and emerging technologies. *Resour. Conserv. Recycl.* **2025**, *215*, 108160. [CrossRef]
2. Zhu, Y.; Jin, Y.; Zhu, J.; Dong, X.; Liu, M.; Sun, Y.; Guo, M.; Li, F.; Guo, F.; Zhang, Q.; et al. Design of N-Type Textured Bi_2Te_3 with Robust Mechanical Properties for Thermoelectric Micro-Refrigeration Application. *Adv. Sci.* **2022**, *10*, 2206395. [CrossRef] [PubMed]
3. Habashi, F. Precious Metals, Refractory Metals, Scattered Metals, Radioactive Metals and Rare Earth Metals. In *Handbook of Extractive Metallurgy*; Wiley: Hoboken, NJ, USA, 1997; Volume 3, pp. 1649–1684.
4. Habashi, F. *Handbook of Extractive Metallurgy Volume 2*; Métallurgie Extractive Québec: Québec City, Québec, Canada, 1997.
5. Makuei, F.M.; Senanayake, G. Extraction of tellurium from lead and copper bearing feed materials and interim metallurgical products—A short review. *Miner. Eng.* **2018**, *115*, 79–87. [CrossRef]
6. Chung, H.; Friedrich, S.; Becker, J.; Friedrich, B. Purification principles and methodologies to produce high-purity tellurium. *Can. Met. Q.* **2024**, *63*, 1626–1642. [CrossRef]
7. Rix, A.J.; Steyl, J.D.T.; Rudman, J.; Terblanche, U.; van Niekerk, J.L. *First Solar's CdTe Module Technology—Performance, Life Cycle, Health and Safety Impact Assessment*; Version: Final-Rev A.; Centre for renewable and sustainable energy studies: Stellenbosch, South Africa, 2015; pp. 1–32.
8. Fraunhofer IWKS Recycling and Long-Term Stability of Thermoelectric and Magnetocaloric Systems (RecycleTEAM). Available online: https://www.recycleteam.de/en.html (accessed on 13 August 2024).
9. Zhang, X.; Xu, W.; Wang, S.; Liu, D.; Deng, P.; Deng, J.; Jiang, W. Research status of recovery of tellurium from cadmium telluride photovoltaic modules. *IOP Conf. Ser. Mater. Sci. Eng.* **2020**, *782*, 022024. [CrossRef]
10. Anderson, C.D. Hydrometallurgical recovery of tellurium dioxide from cadmium telluride photovoltaic manufacturing scrap. *Mining, Met. Explor.* **2012**, *29*, 133–134. [CrossRef]
11. Fthenakis, V.M.; Wang, W. Extraction and separation of Cd and Te from cadmium telluride photovoltaic manufacturing scrap. *Prog. Photovoltaics: Res. Appl.* **2006**, *14*, 363–371. [CrossRef]
12. Fthenakis, V.; Duby, P.; Wenming, W.; Graves, C.; Belova, A. Recycling of CdTe Photovoltaic Modules : Recovery of Cadmium and Tellurium. In Proceedings of the 21st European Photovoltaic Solar Energy Conference, Dresden, Germany, 4–7 September 2006; pp. 2539–2541.
13. Greenwood, N.; Earnshaw, A. *Chemistry of the Elements*, 2nd ed.; Butterworth-Heinemann: Oxford, UK, 1997.
14. Li, Z.; Liu, D.; Zha, G.; Jiang, W.; Huang, D.; Xu, B.; Yang, B. Efficient separation and recovery of tellurium and copper from high-value-added industrial copper telluride slag by a sustainable process. *J. Sustain. Met.* **2023**, *9*, 738–752. [CrossRef]
15. The European Green Deal—European Commission. Available online: https://commission.europa.eu/strategy-and-policy/priorities-2019-2024/european-green-deal_en (accessed on 23 July 2024).
16. Cavaliere, P. Hydrogen in Reduction Processes. In *Hydrogen Assisted Direct Reduction of Iron Oxides*; Springer International Publishing: Cham, Switzerland, 2022; pp. 47–75.
17. Hassan, Q.; Sameen, A.Z.; Salman, H.M.; Jaszczur, M.; Al-Jiboory, A.K. Hydrogen energy future: Advancements in storage technologies and implications for sustainability. *J. Energy Storage* **2023**, *72*, 108404. [CrossRef]
18. Rukini, A.; Rhamdhani, M.A.; Brooks, G.A.; Van den Bulck, A. Metals Production and Metal Oxides Reduction Using Hydrogen: A Review. *J. Sustain. Met.* **2022**, *8*, 1–24. [CrossRef]
19. Gupta, R.; Kumar, V.A.; Khanra, G. Reactive and liquid-phase sintering techniques. In *Intermetallic Matrix Composites*; Elsevier: Amsterdam, The Netherlands, 2018; pp. 303–318. [CrossRef]
20. Yue, M.; Lambert, H.; Pahon, E.; Roche, R.; Jemei, S.; Hissel, D. Hydrogen energy systems: A critical review of technologies, applications, trends and challenges. *Renew. Sustain. Energy Rev.* **2021**, *146*, 111180. [CrossRef]
21. Ishaq, H.; Dincer, I.; Crawford, C. A review on hydrogen production and utilization: Challenges and opportunities. *Int. J. Hydrogen Energy* **2022**, *47*, 26238–26264. [CrossRef]
22. Birich, A.; Marepalli, K.; Wegmann, F.; Chung, H.; Friedrich, B. Anwendungspotentiale von Wasserstoff in der Nichteisen-Metallurgie (Application of Hydrogen in the Non-Ferrous Metallurgy). *Erzmetall- World Metall.* **2024**, *77*, 192–203.
23. Altmannshofer, S.; Eisele, I.; Gschwandtner, A. Hydrogen microwave plasma treatment of Si and SiO_2. *Surf. Coatings Technol.* **2016**, *304*, 359–363. [CrossRef]
24. Li, Z.Y.; Yu, K.; Gao, Y.; Liu, J.; Jin, D.; Zhai, Y.C. Effect of Particle Size on Hydrogen Reduction Reaction Kinetics Parameters of Cu_2O Powders. *Mater. Sci. Forum* **2011**, *694*, 769–772. [CrossRef]
25. Hidayat, T.; Rhamdhani, M.; Jak, E.; Hayes, P. The Kinetics of Reduction of Dense Synthetic Nickel Oxide in H_2-N_2 and H_2-H_2O Atmospheres. *Met. Mater. Trans. B* **2009**, *40*, 1–16. [CrossRef]
26. Dang, J.; Zhang, G.-H.; Chou, K.-C.; Reddy, R.G.; He, Y.; Sun, Y. Kinetics and mechanism of hydrogen reduction of MoO_3 to MoO_2. *Int. J. Refract. Met. Hard Mater.* **2013**, *41*, 216–223. [CrossRef]

27. Keilholz, S.; Paul, R.; Dorsch, L.Y.; Kohlmann, H. In Situ X-ray Diffraction Studies on the Reduction of V_2O_5 and WO_3 by Using Hydrogen. *Chem. A Eur. J.* **2023**, *29*, e202203932. [CrossRef]
28. Altay, M.C.; Eroglu, S. H_2-mediated reduction of GeO_2 and chemical vapor deposition of polycrystalline Ge porous films. *Thin Solid Films* **2023**, *783*, 140049. [CrossRef]
29. Trawiński, B.; Bochentyn, B.; Kusz, B. A study of a reduction of a micro- and nanometric bismuth oxide in hydrogen atmosphere. *Thermochim. Acta* **2018**, *669*, 99–108. [CrossRef]
30. Kim, B.-S.; Lee, J.-C.; Yoon, H.-S.; Kim, S.-K. Reduction of SnO_2 with Hydrogen. *Mater. Trans.* **2011**, *52*, 1814–1817. [CrossRef]
31. Hovestadt, G.; Coldewe, M.; Friedrich, B. Determining critical parameters of hydrogen reduction treatment of low copper-containing primary slags. In Proceedings of the European Metallurgical Conference 2023, Düsseldorf, Germany, 11–14 June 2023; pp. 1–7. [CrossRef]
32. Kar, M.K.; van der Eijk, C.; Safarian, J. Kinetics Study on the Hydrogen Reduction of Bauxite Residue-Calcite Sintered Pellets at Elevated Temperature. *Metals* **2023**, *13*, 644. [CrossRef]
33. Qu, G.; Wei, Y.; Li, B.; Wang, H.; Yang, Y.; McLean, A. Distribution of copper and iron components with hydrogen reduction of copper slag. *J. Alloys Compd.* **2020**, *824*, 153910. [CrossRef]
34. Tang, J.; Chu, M.-S.; Li, F.; Feng, C.; Liu, Z.-G.; Zhou, Y.-S. Development and progress on hydrogen metallurgy. *Int. J. Miner. Met. Mater.* **2020**, *27*, 713–723. [CrossRef]
35. Luidold, S.; Antrekowitsch, H. Hydrogen as a reducing agent: State-of-the-art science and technology. *JOM* **2007**, *59*, 20–26. [CrossRef]
36. Trawiński, B.; Bochentyn, B.; Łapiński, M.; Kusz, B. A study of the kinetics of bismuth telluride synthesis by an oxide reduction method. *Thermochim. Acta* **2020**, *683*, 178437. [CrossRef]
37. Trawiński, B.; Kusz, B. Kinetic analysis of the reduction of a ternary system of Bi, Sb and Te oxides by hydrogen for $BiSbTe_3$ synthesis. *Thermochim. Acta* **2021**, *701*, 178966. [CrossRef]
38. Peray, K.E. *The Rotary Cement Kiln*, 2nd ed.; Arnold: London, UK, 1986.
39. Boateng, A.A. *Rotary Kilns: Transport Phenomena and Transport Processes*; Elsevier: Amsterdam, The Netherlands, 2016.
40. Avrami, M. Kinetics of Phase Change. II Transformation-Time Relations for Random Distribution of Nuclei. *J. Chem. Phys.* **1940**, *8*, 212–224. [CrossRef]
41. Pöyhtäri, S.; Ruokoja, J.; Heikkinen, E.-P.; Heikkilä, A.; Kokkonen, T.; Tynjälä, P. Kinetic Analysis of Hydrogen Reduction of Nickel Compounds. *Met. Mater. Trans. B* **2023**, *55*, 251–265. [CrossRef]